On-Body Transmission at 5.2 GHz: Simulations Using FDTD With a Time Domain Huygens' Technique

Sema Dumanli, *Member, IEEE*, and Chris J. Railton, *Member, IEEE*

***Abstract*—On-body communications systems are heavily influenced by the effects of the human body and cannot be analyzed without taking these into account. This, however, leads to a large problem which is a challenge to model. In this paper a transmission scenario is modeled which includes transmit and receive cavity backed slot (CBS) antennas on the body of a male adult. The slots are backed with cavities in order to get unidirectional radiation patterns and decrease the near field body interaction of the slots. The scenario is simulated with finite difference time domain (FDTD) method in combination with a time domain Huygens' (TDH) technique in order to reduce the computational load. A cylindrical numerical phantom including 15 different tissue types is modeled to represent the upper body of a male. The predicted transmission coefficient, return loss and radiation patterns obtained using the TDH method are shown to be in agreement with the resource intensive direct FDTD approach but are obtained in approximately 30% of the time.**

***Index Terms*—Finite difference time domain technique, Huygens' technique, on-body transmission, slot antenna.**

I. Introduction

LINKS in a Body Area Network (BAN) can be classified into three categories: off-body, on-body and in-body links [1]. On-body links are the links in between the antennas on the body which might be used for medical or non-medical applications. Possible medical applications include monitoring heart rate, blood pressure, temperature and respiration [2]. Gaming, establishing social network and assessing soldier fatigue are among the non-medical applications [3]. On body antenna design is a challenging task due to the body being in the near-field of the antenna and the complex interaction between the two. In addition to the taking account of the influence of the body on the antenna characteristics, the propagation channel should be modeled carefully in order to ascertain the transmission link efficiency and to predict possible coverage problems and limitations of the maximum data rate due to the delay spread.

Manuscript received December 06, 2010; revised February 18, 2011; accepted April 04, 2011. Date of publication August 08, 2011; date of current version October 05, 2011.

S. Dumanli is with Toshiba Research Europe Ltd., Bristol BS1 4ND, U.K. (e-mail: sema.dumanli@toshiba-trel.com).

C. J. Railton is with the Centre for Communications Research, University of Bristol, Bristol BS8 1UB, England, (e-mail: chris.railton@bristol.ac.uk).

Color versions of one or more of the figures in this paper are available online at http://ieeexplore.ieee.org.

Digital Object Identifier 10.1109/TAP.2011.2163786

On-body radio channel scenarios can be characterized experimentally [4], [5] as well as computationally. A number of methods are available for modeling propagation channels such as this, e.g., [6]. However, the FDTD method is most often used to predict on-body propagation since its capability of modeling inhomogeneous materials [7] facilitates the accurate modeling of the body. Moreover, the flexibility of the method allows the detailed geometry of the antennas and the propagation environment to be readily included. Generally measurements are chosen over simulations due to their being able to include the full effects of practical small antennas being placed near the body. Simulations, on the other hand, are generally limited to simple scenarios since the run time becomes impractically long for large and detailed problems. In those cases, however, they are cheaper and less time consuming [4]. A means of reducing the computational requirements for more complicated problems would therefore yield many benefits.

Much of the difficulty arises from the fact that the antenna elements contain much fine detail which necessitates a dense mesh while the complete propagation channel is electrically large. This combination leads to a very large number of cells and the necessity for a very small time step. A number of techniques have been proposed in the literature in order to overcome the computational complexity of these multi-scale simulations including sub-gridding [8] and dual grid FDTD [9]. Sub-gridding is based on using a small step size only around small structures and using a large step size elsewhere. It is successful in reducing the run time however it is prone to numerical instability and to spurious reflections from the grid sub-grid interface.

Dual grid FDTD deals with multi-scale structures by running two or more separate simulations. Small detailed structures are modeled with a fine grid while the larger part of the structure is modeled with a coarse grid. The different simulations are linked using Huygens surfaces. In [10] this method is applied to a simple propagation channel together with the two antennas. The computational complexity was overcome by dividing the problem domain into three sub-domains. These domains are combined by means of Huygens' Principle which is applied in time domain in order to preserve delay profile information in a direct manner. Dual grid FDTD has also been applied to on-body transmission analysis in [11]. In that paper a homogenous partial body model was used to calculate the transmission coefficient between two antennas but no time domain data or radiation patterns were presented. In this work, a similar approach is taken but with a more detailed body model and a more flexible algorithm for the interpolation of the fields.

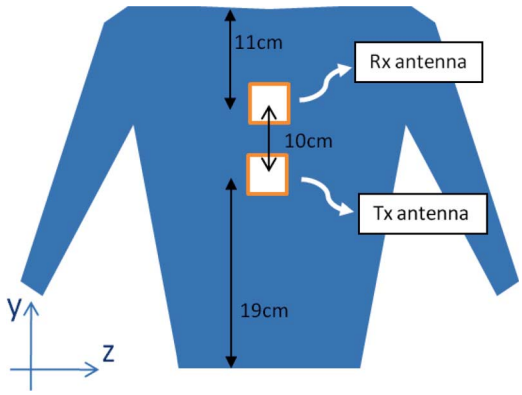

Fig. 1. Two CBS antennas, one transmit and one receive, located on the upper body of a male.

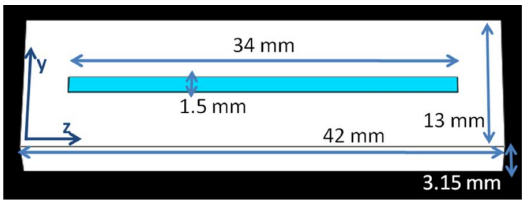

Fig. 2. Geometry of the CBS antenna.

Also, in this work, graded meshes are used wherever appropriate in order to further improve efficiency. In addition, the antenna modeled here is a slot antenna which means the Huygens surface need only cover the slot rather than having to enclose the complete antenna structure and the singular behavior of the field within the slot can be accounted for by an analytical correction factor which allows a coarser mesh to be used while maintaining accuracy. In order to demonstrate that this TDH method is accurate and efficient, the complete link including the antennas is also modeled by a direct FDTD simulation. It is shown that, by using the TDH method, a time saving of approximately 70% can be achieved with little loss in accuracy. For larger problems the savings would be greater.

A layered upper body model is used and transmission channel is characterized in both the time and frequency domain. The influence of the body on the antenna characteristics is also presented while demonstrating the performance of the improved FDTD technique on body influence.

The paper starts with a detailed explanation of the propagation scenario. Antenna elements and the numerical body phantom are described in Section II. In Section III, FDTD simulations improved with the TDH technique (FDTD-TDH) is discussed. Section IV presents the interpolation schemes used in TDH. The performance of direct FDTD simulations and FDTD-TDH with different interpolation schemes are compared in terms of transmission coefficients and the individual antenna properties in Section V. The influence of the body on the frequency response and the radiation pattern of the transmit antenna is also presented. Finally the paper concludes in Section VI.

TABLE I
ELECTRICAL PROPERTIES OF THE BODY TISSUES

Tissue Type	Relative Permittivity	Conductivity (s/m)	Penetration depth (mm)
Body Fluid	65.56	5.71	7.6
Bone Cortical	9.95	1.01	16.8
Bone Marrow	5.02	0.25	48.5
Cerebro Spinal Fluid	61.59	6.90	6.1
Colon	49.41	4.82	7.8
Fat	5.01	0.26	46.8
Heart	49.94	5.11	7.5
Kidney	47.73	5.18	7.2
Liver	38.98	4.03	8.4
Lung Inflated	18.85	1.81	12.9
Muscle	49.28	4.27	8.8
Skin Dry	35.61	3.22	10
Small Intestine	49.65	6.00	6.4
Spinal Chord	27.72	2.55	11.1
Stomach	57.54	5.44	7.5

II. ON-BODY PROPAGATION SCENARIO

A transmit and a receive antenna is located on the upper body of a male as seen in Fig. 1. The distance between the antennas is 10 cm and the distance between the back of the CBS antennas and the body is $5\ \mathrm{mm}(=0.087\lambda)$.

The propagation characteristics are investigated at 5.2 GHz. The antennas used in the scenario are described in the next subsection.

A. Antenna Element

A slot antenna backed with a shallow cavity and fed with a stripline is used as the antenna element [12]. The slot is a half wavelength narrow slot operating at 5.2 GHz. The cavity is filled with a dielectric substrate having a relative permittivity of 2.2. The overall dimensions of the antenna are $42 \times 13 \times 3.15\ \mathrm{mm}$. The antenna element was designed and analyzed by FDTD simulations. Fig. 2 shows the dimensions of the modeled antenna.

B. Numerical Body Phantom

Different numerical phantoms have been reported in the literature so far. These range from flat uniform models [13]–[15] to voxel models generated with the help of precise MRI measurements [16]. Here an upper body of an average male excluding the head is modeled as a cylindrical multi-layered structure using 15 different tissue types. The body parts and organs are approximated by basic geometries such as spheres, cylinders and cubes. Considering that the physical properties of individuals vary drastically, an average model is more appropriate to use for a generic channel simulation. In addition the human body is very lossy and the penetration depth is very small at 5.2 GHz therefore the detailed inner body parts have little effect on the channel. The thickest outermost layer of the model is muscle tissue with 20 mm thickness. As shown in Table I, the penetration depth of the muscle is less than 9 mm. This effect will be demonstrated in detail in Section V. Permittivity and conductivity values of the tissues are calculated for 5.2 GHz [16], [17] and listed in Table I.

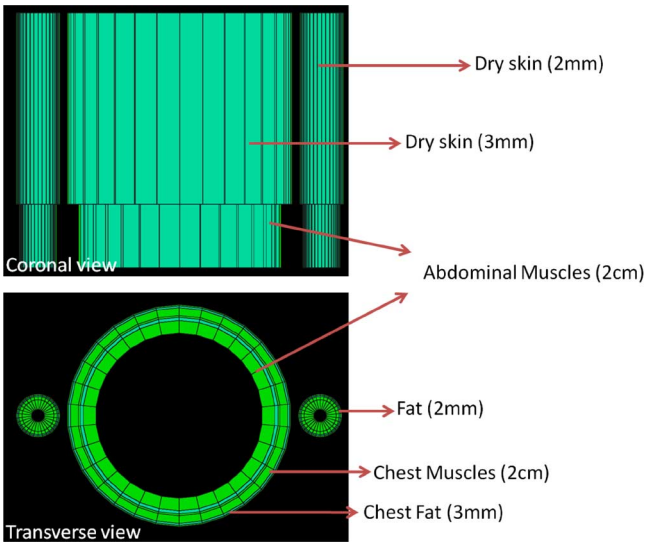

Fig. 3. Outer layers of the body showing skin (thickness (t): 2 mm in the arms and 3 mm in the chest and abdomen), fat (t: 2 mm in the arms and 3 mm in the chest and abdomen) and muscle (t: 2 cm) layers in coronal and transverse view.

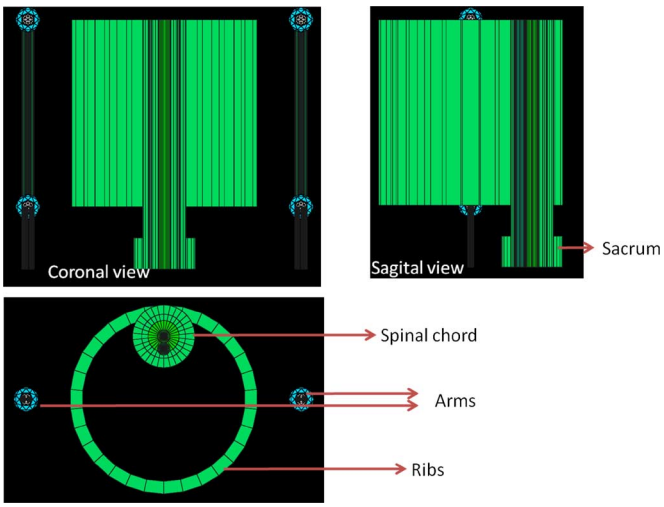

Fig. 4. Bones: humerus (radius(r):1, length(l): 30 cm), radius (r:0.5, l:10 cm), ulna (r:0.4, l:10 cm), spinal column (l: 40 cm), ribs (l: 30 cm) and sacrum (l:5 cm).

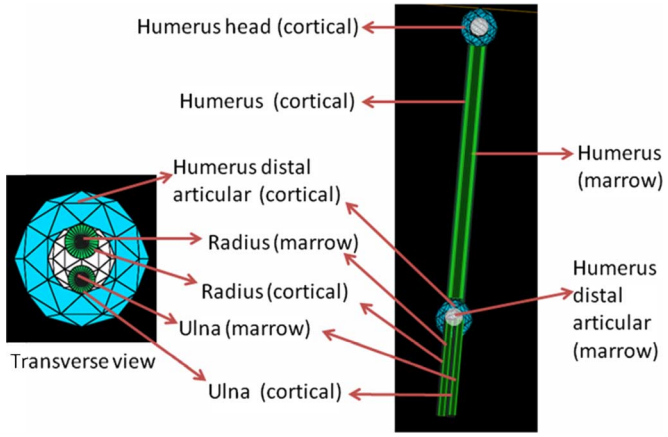

Fig. 5. Bones of the arm: humerus head (r: 2 cm), humerus distal articular (r: 2 cm).

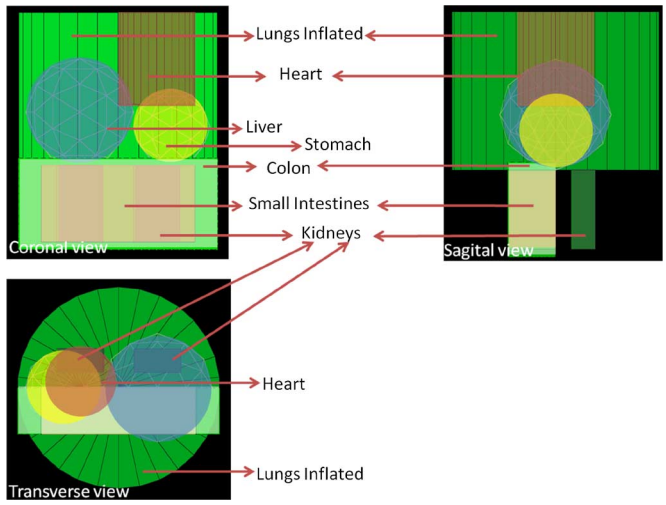

Fig. 6. Organs: lungs (cylinder r: 13, l: 20 cm), heart (cylinder r: 5, l: 12 cm), liver (sphere r: 7 cm), stomach (sphere r: 5 cm), colon (block $6 \times 12 \times 26$ cm), small intestines (block $6 \times 10 \times 20$ cm), kidneys (block $3 \times 6 \times 10$ cm).

Fig. 3 shows the outermost layers of the cylindrical structure. The skin is assumed to be dry and taken as 3 mm thick for the chest and abdomen and 2 mm thick for the arms. Fat thickness is the same as the skin thickness and all the muscles are taken to be 2 cm thick [18].

The bones: Humerus, Radius, Ulna, Ribs, Sacrum and Spinal column are defined with 2 tissue types: the cortical and the marrow as seen in Fig. 4 and Fig. 5. Typical dimensions of the bones are taken from [19]. The Spinal Cord and the Cerebro Spinal Fluid are introduced in the Spinal Column in addition to the Spinal Column marrow.

The inner body parts such as body fluid and organs are also included. Fig. 6 shows the diagram of the organs.

As previously mentioned, the penetration depth at this frequency is very small and the inner body parts are expected to have very little effect on the performance of the antennas. To confirm this, two body models are used here. Body Model A does not include the arms and the organs. Body Model B is the detailed body model including all the body parts described above. Simulations with Model A and B are performed and the effects are presented in Section V.

III. Time Domain Huygens' Technique

In order to reduce the amount of computer resources needed to analyze this huge problem which would require 49 million FDTD cells for the direct approach, it is split into three stages using the approach described in [10].

A. First Stage

In this stage the transmit antenna is modeled in isolation. Only the immediate vicinity of the antenna need be included so that the computational domain is much smaller than would be needed to model the complete scenario. In this case the computational domain is $72 \times 81 \times 100$ mm and a fine mesh is used consisting 5 million FDTD cells. The smallest cell size is 0.2 mm$(= 0.0035\lambda)$ and the largest cell size is 1.5 mm$(=$

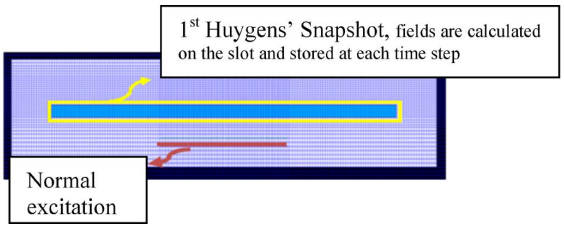

Fig. 7. First step, the transmit antenna with a Huygens' snapshot, Huygens' surface is labeled with the yellow box.

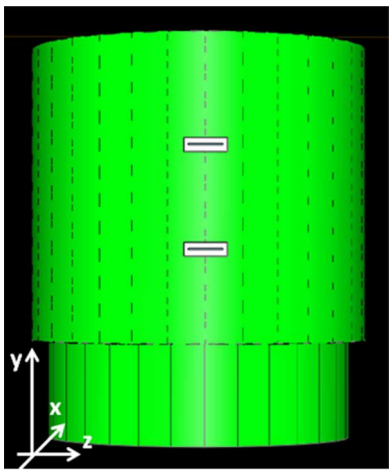

Fig. 8. The whole scenario is simulated with coarse mesh using the Huygens' excitation, body model A is used for these simulations.

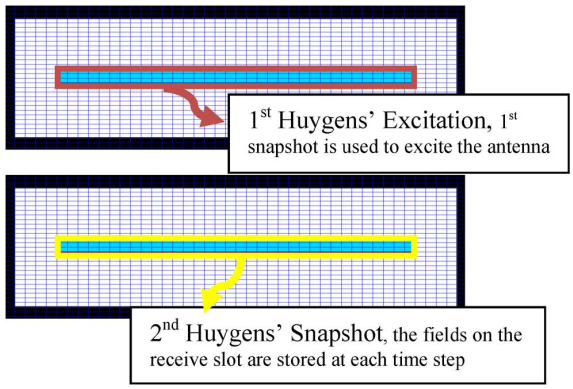

Fig. 9. The excitation of the transmit antenna and the Huygens' snapshot on the receive antenna at second stage.

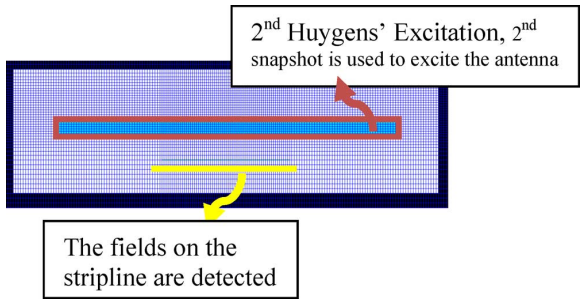

Fig. 10. Final stage, the receive antenna is excited with the Huygens' snapshot generated in the second stage.

0.026λ). The antenna is excited with a current source applied to the stripline feed.

During the FDTD run, a Huygens' snapshot, positioned as shown in Fig. 7, is stored to a computer file for use in stage 2. This is done by recording the tangential electric and magnetic fields at each time step and on each FDTD node in the slot.

In order to check whether near body interaction would cause significant coupling through the slot and therefore affect the recorded snapshot, this stage was rerun with part of the human body included. The region of the body which is included has dimensions $0.5\lambda \times 1\lambda \times 1\lambda$ (half wavelength into the body). It was found that the results were almost identical to those obtained with the body excluded. This would be expected since the radiation from the CBS antenna is largely directed away from the body.

B. Second Stage

For this stage, the complete link, including the two antennas and the human body, is simulated with a coarse mesh as shown in Fig. 8. The antenna no longer needs to be covered with fine mesh, since the structure is excited with the previously generated Huygens' snapshot. This decreases the number of FDTD cells which would be needed from 49 million to less than 22 million. The mesh still has to be fine enough to accurately model the slot. Here three different cases are considered where the width of the slot is modeled with 1, 2 or 3 FDTD cells. The cell sizes are, 1 mm($= 0.017\lambda$), 0.75 mm($= 0.013\lambda$) and 0.5 mm($= 0.0087\lambda$) respectively. Run time and accuracy increase as the cell size decreases.

During the second stage, the fields on the receiver antenna's slot are also stored in another Huygens' snapshot to be used in the last stage as seen in Fig. 9.

C. Third Stage

Finally the receiver antenna is modeled in isolation using a similar mesh to the one used for stage 1. The human body is not included at this stage and the computational domain is small. In this case the antenna is excited using the Huygens' snapshot generated in the second stage as seen in Fig. 10. The output is then taken from the antenna feed line. This stage uses 5 million FDTD cells.

IV. Interpolation Schemes

In the scheme described above, it is necessary to store a Huygens snapshot during the running of Stage 1 and to use this snapshot as an excitation source in Stage 2. Similarly it is necessary to store a Huygens snapshot during the running of Stage 2 and to use this snapshot as an excitation source in Stage 3. Since the time step and cell sizes are different in the different stages, it is necessary to perform an interpolation in space and time. There are a number of ways in which this may be done.

For the Huygens snapshot generated in Stage 1, the tangential E and H fields on the aperture of the slot antenna are recorded. Because the aperture is placed on the TE plane of the FDTD mesh, the values of the H field are obtained by averaging the values of H on the nodes which are half a cell size on either side of the aperture plane. Because the time step in Stage 2 is greater than that of Stage 1 it is not necessary to record the fields

TABLE II
COMPARISON OF DIRECT FDTD SIMULATIONS WITH THE ONES IMPROVED WITH HUYGENS' TECHNIQUE

	Run Time (mins)	Smallest cell size (λ)	Largest cell size (λ)	Problem Dimensions
Direct FDTD	1200	0.004	0.052	48705
1st stage FDTD-TDH	57	0.004	0.026	5238
2nd stage FDTD-TDH (3 cells) Interpolation A / Interpolation B	368 / 392	0.009	0.052	21806
2nd stage FDTD-TDH (2 cells) Interpolation A / Interpolation B	275 / 300	0.013	0.052	19051
2nd stage FDTD-TDH (1 cell) Interpolation A / Interpolation B	201 / 219	0.017	0.052	15388
3rd stage FDTD-TDH Interpolation A / Interpolation B	118 / 126	0.004	0.026	5238
FDTD-TDH Total (2 cells) Interpolation A / Interpolation B	450 / 483	-	-	-
FDTD-TDH Total (1 cell) Interpolation A / Interpolation B	376 / 402	-	-	-

at every time step. The time interpolation is done using a linear interpolation in a similar manner to that done in [11].

Following the time interpolation, the snapshot is interpolated in space from the source mesh to the target mesh. Two different schemes are considered in this paper and their performance compared.

A. Linear Interpolation Onto Each Target Node

Details of this scheme are given in [9] which is similar to that used in [11]. Here the equivalent current at each node on the target FDTD mesh is estimated from the nearest eight source nodes using a tri-linear interpolation. The equivalent currents are then included in the update equations for the target node.

B. Interpolation From Each Source Node

As an alternative to the above, the source snapshot can be treated as a grid of wires which carry the equivalent electric and magnetic currents. The methods which exist for incorporating thin wires into the FDTD grid, e.g., [20]–[22] can then be used here. For this application, however, the excitation is one-way since there is no influence of the fields in the FDTD mesh upon the equivalent wires.

A popular thin wire scheme was introduced by Holland and Simpson [20]. In this scheme the current at each node in the snapshot is shared out amongst the eight nearest target nodes in accordance with a tri-linear interpolation scheme. It was shown, however, that this method of is not accurate when the wires are not coincident with the FDTD mesh and that improved performance can be achieved by sharing out the currents over a greater number of FDTD nodes using a "shell average" interpolation [21], [22]. Because of this spreading of the current distribution, the scheme is less affected by the exact position of the wires.

This method of interpolation has the advantage that it opens the door to the use of Huygens surfaces which are tilted with respect to the FDTD mesh which the method described in the previous section does not. This is important as it allows the modeling of scenarios where the transmit and receive antennas are not in the same plane and therefore cannot be efficiently analyzed with a single Cartesian coordinate system. The application to this type of situation is the subject of ongoing research.

V. RESULTS AND DISCUSSION

A. Performance of the FDTD-TDH Simulations

In this section, results are presented for the example scenario with the use of the two interpolation schemes described in the previous Section. In addition, the effect of different choices of cell sizes in Stage 2 is shown. All the simulations are performed on Intel Xeon X5670 @2.93 GHz processor. The run time for the 1st stage is 57 minutes. Total time spent during the 2nd stage changes between 392 and 201 minutes depending on the cell size and the chosen interpolation scheme. Finally the 3rd stage takes 118 minutes with Interpolation A and 126 minutes with Interpolation B. In total the FDTD-TDH takes 376 and 402 minutes respectively as summarized in Table II. This is just 31.3% of the time needed for the direct run. In addition, the first stage need only be run once if a number of different positions of the antennas are required to be modeled as long as the same antenna element is used. Note that although the time elapsed with Interpolation B is a little longer than Interpolation A, however, interpolation B allows Huygens' surfaces which are tilted with respect to with the FDTD mesh whereas interpolation A as used in [11] does not.

1) Transmission Characteristics: The transmitter and receiver are located on Body Model A. The transient response as seen in the feed line of the receive antenna obtained by direct FDTD simulations and by FDTD-TDH are plotted in Fig. 11 and Fig. 12. It can be seen that the response predicted by FDTD-TDH is much lower than the results predicted by direct FDTD simulations when the Huygens' snapshot is covered with only 1 cell for each interpolation scheme. However there is not much difference between the 2 and 3 cells cases. The overall response of FDTD-TDH is similar to direct FDTD although the magnitude of the transient response is underestimated. The results obtained with Interpolation B are similar to Interpolation

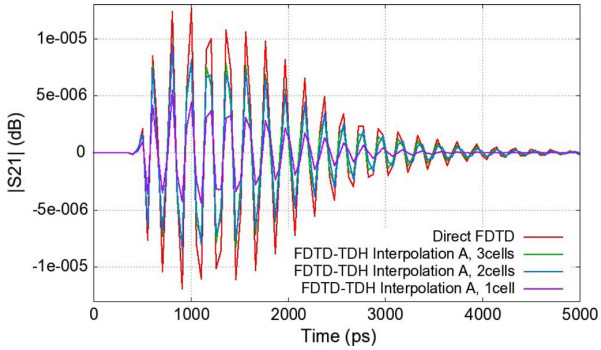

Fig. 11. Transient response of body model A as seen in the feed line of the receive antenna obtained by direct FDTD simulations and FDTD-TDH with interpolation A.

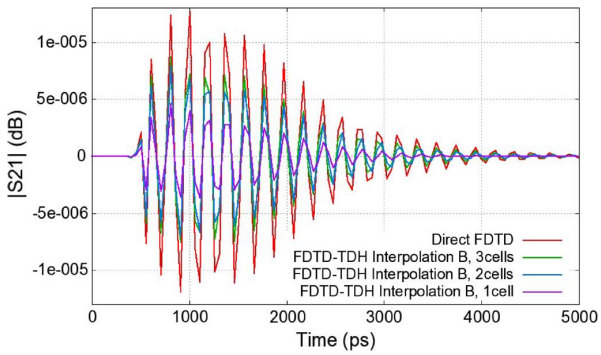

Fig. 12. Transient response of body model A as seen in the feed line of the receive antenna obtained by direct FDTD simulations and FDTD-TDH with interpolation B.

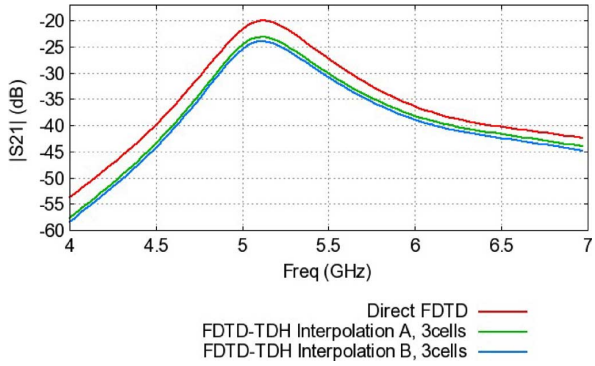

Fig. 13. S21 of body model A predicted by direct FDTD simulations and FDTD-TDH with Interpolation A & interpolation B.

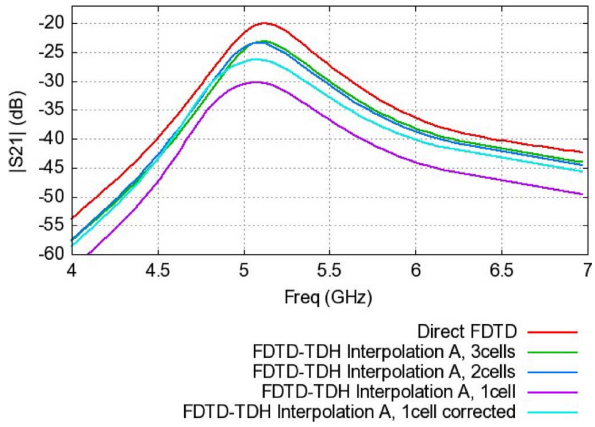

Fig. 14. S21 of body model A predicted by direct FDTD simulations and FDTD-TDH with interpolation A with different mesh.

A but interpolation B has the advantage that it can be used for future applications which include tilted antennas.

The results for 1 cell can be improved by recognizing that the field in the slot will exhibit a singularity at the metal edges as shown in (1)

$$E_y \propto \frac{1}{\sqrt{y^2 - \left(\frac{w}{2}\right)^2}} \tag{1}$$

where w is the width of the slot and the origin is taken as the slot center.

If only one cell is used to approximate this field then the total effect will be underestimated because the FDTD algorithm will assume that the E field is constant across the width of the slot. This can be corrected for by multiplying the field by a factor of

$$\frac{2}{w}\int_{-\frac{w}{2}}^{\frac{w}{2}} \frac{dy}{\sqrt{y^2 - \left(\frac{w}{2}\right)^2}} = \frac{\pi}{2}. \tag{2}$$

Correcting in this way will bring the result close to that obtained using a finer mesh.

The frequency domain results generated using the signals at the antenna ports can be seen in Fig. 13 and Fig. 14. Fig. 13 shows that both interpolation techniques give almost identical results while there is approximately 3 dB difference between the direct FDTD and FDTD-TDH with 3 cells. The reason for this discrepancy is under investigation. The results generated by FDTD-TDH with interpolation A are plotted in Fig. 14 for 3 cells, 2 cells, 1 cell and "1 cell with the correction." It can be seen that decreasing the number of cells from 3 cells to 2 cells does not have much effect while the correction factor improves the 1 cell case.

The variation of channel characteristics, based on measurements done by the authors, indicates that there can be variations of up to 7 dB between one person and another. The 3 dB discrepancy here is comfortably less than this and so, while it is not ideal, does give acceptable and useful results.

2) Radiation Patterns: The radiation patterns obtained with direct FDTD simulations and from the 2nd stage of the FDTD-TDH can be seen in Fig. 15. The 3D radiation patterns are plotted in a relative dB scale where the center of the plot corresponds to -20 dB. The plots look identical while the calculated radiation pattern correlation at 5.2 GHz is 99% showing very good agreement between the direct FDTD and the FDTD-TDH approaches.

This quantity is defined as

$$R_{ij} = \frac{W_{ij}}{\sqrt{W_{ii}W_{jj}}} \tag{3}$$

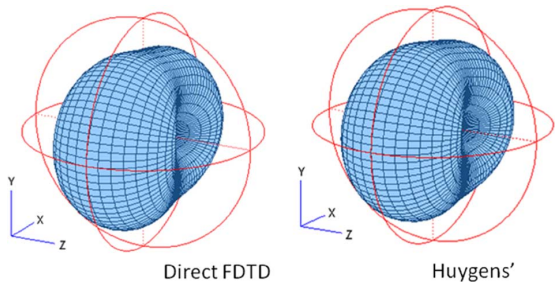

Fig. 15. Radiation pattern of the transmit antenna on the body model A at 5.2 GHz, predicted with direct FDTD simulations and FDTD-TDH.

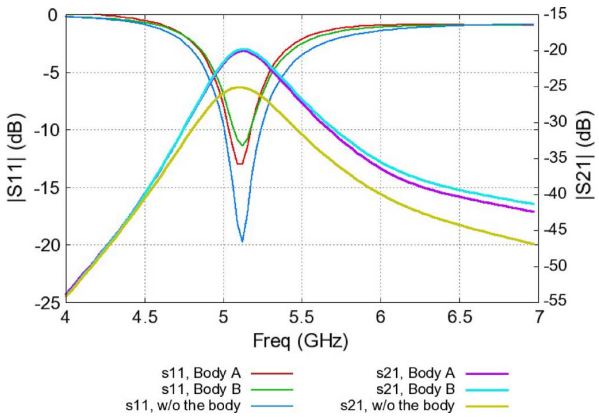

Fig. 16. S11 and S21 predicted **by direct FDTD** simulations when the antenna is located on body model A, body model B and when there is no body model.

where

$$W_{ij} = \int_0^{2\pi} \int_0^{\pi} E_\theta^i(\theta,\varphi)\overline{E_\theta^j(\theta,\varphi)}\sin(\theta)d\theta d\phi \qquad (4)$$

and $\mathrm{E^i}$ is the E field radiation of the ith pattern.

The improved technique is very powerful in predicting the radiation patterns and can be used to find out the body influence on the antenna characteristics without the need for a fine mesh and a long run.

B. Body Influence on the Antenna Analyzed by Direct FDTD

The reflection coefficient of the antenna predicted by direct FDTD simulations is plotted in Fig. 16. The magnitude of $\mathrm{S_{11}}$ at the operating frequency decreases when the antenna is located on the body. This is because of the lossy nature of the body tissues. No detuning is observed, however, which indicates that the CBS antenna is a good candidate for on Body communications. The $\mathrm{S_{11}}$ characteristics of the antennas on Body Model A and B agree very well since the penetration depth is very short and the inner body parts do not have much effect.

The transmission coefficient is plotted in Fig. 16. $\mathrm{S_{21}}$ between the antennas agree well for the case of Body model A and Body model B however the magnitude of the transmission coefficient is approximately 5 dB less when there is direct transmission between the antennas without (w/o) the body model. -25 dB is an expected result as the free space loss is around -25 dB and the antenna directivities in y direction ($\theta = \pm 90$, $\varphi = 90$) are 0 dB. The transmission coefficient is in the order of -20 dB when the antennas are located on the body models. This is due to the surface waves. The transmission is not free-space transmission anymore but supported by the surface waves on the body.

Radiation patterns of the transmit antenna on Body Model A and B also are very similar and the correlation is 99%. This is another implication of the inner body parts being insignificant at this operating frequency.

VI. Conclusion

An on-body communications link with a cylindrical layered phantom is analyzed by means of the FDTD-TDH technique. It is shown that by splitting the problem into three parts and using TDH, 68.7% decrease in the run time is observed compared to a direct FDTD run. The technique is shown to be very powerful for modeling inhomogeneous media and small objects and details as well as promising the possibility of inclusion of tilted antennas in future applications. The body influence on the antenna characteristics is also monitored using the same technique in a much shorter time. The operating frequency and the radiation characteristics of CBS antenna are shown to be insensitive to the body therefore the CBS is proven to be suitable for this type of application.

Acknowledgment

The authors would like to thank to their colleagues in the Communication Systems and Networks Group, headed by Prof. J. McGeehan for helpful discussions.

References

[1] P. S. Hall and Y. Hao, "Antennas and propagation for body centric communications," presented at the Eur. Conf. on Antennas Propag. (EuCAP 2006), Nice, France, 2006.

[2] P. Khan, A. Hussain, and K. S. Kwak, "Medical applications of wireless body area networks," *Int. J. Digital Content Technol. Its Applicat,*, vol. 3, no. 3, Sep. 2009.

[3] S. Ullah, P. Khan, N. Ullah, S. Saleem, H. Higgins, and K. S. Kwak, "A review of wireless body area networks for medical applications," *Int. J. Commun., Netw. Syst. Sci. (IJCNS)*, vol. 2, no. 8, pp. 798–803, Jul. 2009.

[4] A. Fort, C. Desset, P. D. Doncker, P. Wambacq, and L. V. Biesen, "An ultra-wideband body area propagation channel model—From statistics to implementation," *IEEE Trans. Microwave Theory Tech.*, vol. 54, no. 4, Apr. 2006.

[5] A. Sani, Y. Zhao, A. Alomainy, Y. Hao, and C. Parini, "Modelling of propagation and intereaction between body-mounted antennas, and the modelling of body-centric, context aware application scenarios," *Antennas Propag. Body-Centric Wireless Commun.*, pp. 1–6, Apr. 2009.

[6] T. Sasamori, M. Takahashi, and T. Uno, "Transmission mechanism of wearable device for on-body wireless communications," *IEEE Trans. Antennas Propag.*, vol. 57, no. 4, pp. 943–955, Apr. 2009.

[7] Y. Zhao, Y. Hao, and C. Parini, "Two novel FDTD based UWB indoor propagation models," in *Proc. IEEE Int. Conf. on Ultra-Wideband*, Sep. 2005, pp. 124–129.

[8] S. S. Zivanovic, K. S. Yee, and K. K. Mei, "A subgridding method for the time-domain finite-difference method to solve Maxwell's equations," *IEEE Trans. Microwave Theory Tech.*, vol. 39, no. 3, pp. 471–479, Mar. 1991.

[9] R. Pascaud, R. Gillard, R. Loison, J. Wiart, and M. F. Wong, "Dual-grid finite-difference time-domain scheme for the fast simulation of surrounded antennas," *IET Microw. Antennas Propag.*, vol. 1, no. 3, pp. 700–706, 2007.

[10] S. Dumanli, C. J. Railton, and D. L. Paul, "FDTD channel modeling with time domain Huygens' technique," in *Proc. 5th Eur. Conf. on Antennas Propag.*, Apr. 11–15, 2011, pp. 86–89.

[11] C. Miry, R. Loison, and R. Gillard, "An efficient bilateral dual-grid-FDTD approach applied to on-body transmission analysis and specific absorption rate computation," *IEEE Trans. Microwave Theory Tech.*, vol. 58, no. 9, Sept. 2010.
[12] S. Dumanli, C. J. Railton, D. L. Paul, and G. S. Hilton, "Closely spaced array of cavity backed slot antennas with pin curtain walls," *IET Microw. Antennas Propag.*, vol. 5, no. 1, pp. 38–47, Jan. 2011.
[13] C. M. Weil, "Absorption characteristics of multilayered sphere models exposed to UHF/microwave radiation," *IEEE Trans. Biomed. Engrng.*, vol. 22, no. 6, pp. 468–476, 1975.
[14] H. Massoudi, "Electromagnetic absorption in multilayered cylindrical models of man," *IEEE Trans. Microwave Theory Tech.*, vol. 27, no. 10, pp. 825–830, 1979.
[15] S. Nishizawa and O. Hasimoto, "Effective shielding analysis for three layered human model," *IEEE Trans. Microwave Theory Tech.*, vol. 47, no. 3, pp. 277–283, 1999.
[16] T. Nagaoka1, S. Watanabe, K. Sakurai, E. Kunieda, S. Watanabe1, M. Taki, and Y. Yamanaka, "Development of realistic high-resolution whole-body voxel models of Japanese adult males and females of average height and weight, and application of models to radio-frequency electromagnetic-field dosimetry," *Phys. Med. Biol*, vol. 49, no. 1, Jan. 2004.
[17] "Calculation of Dielectric Properties of Body Tissues in the Frequency Range 10 Hz–100 GHz," Italian Research Council [Online]. Available: http://niremf.ifac.cnr.it/tissprop/htmlclie/htmlclie.htm#atsftag
[18] R. Augustine, "Electromagnetic modelling of human tissues and its application on the interaction between antenna and human body in the BAN context," Thesis submitted to University of Paris, Jul. 2009 [Online]. Available: http://tel.archives-ouvertes.fr/docs/00/49/92/55/PDF/2009PEST1006_0_0.pdf
[19] "E Skeletons Project," University of Texas at Austin [Online]. Available: http://www.eskeletons.org/index.html
[20] R. Holland and L. Simpson, "Finite-difference analysis of EMP coupling to thin struts and wires," *IEEE Trans. Electromagn. Compat.*, vol. EMC-23, pp. 88–97, 1981.
[21] G. Ledfelt, "Hybrid time-domain methods and wire models for computational electromagnetics," Ph.D. dissertation, Dept. Numer. Analy. Comput. Sci., Royal Institute of Technology, Stockholm, 2001.
[22] G. Ledfelt, "A stable subcell model for arbitrarily oriented thin wires for the FDTD method," *Int. J. Numer. Model.: Electron. Networks, Devices Fields*, no. 15, pp. 503–515, 2002.

Sema Dumanli (M'11) was born in Elazig, Turkey, in 1984. She received the B.Sc. (Hons) degree in electrical and electronic engineering from Middle East Technical University (METU), Ankara, Turkey, in 2006 and the Ph.D. degree from the University of Bristol, Bristol, U.K., in 2010.

She had worked at ASELSAN Inc., Turkey, from 2006 to 2007, as a Design Engineer. She currently works at Toshiba Research Europe, Bristol, U.K., as a Research Engineer. Her research interests include antenna design and propagation channel modeling, for the applications to MIMO, mm-wave technology and BAN.

Dr. Dumanli was the recipient of the Scientific and Technological Research Council of Turkey (TUBITAK) Ph.D. Scholarship and Ph.D. sponsorship of Toshiba Research Europe.

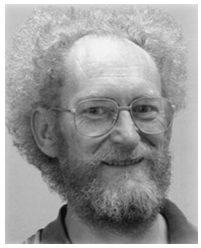

Chris J. Railton (M'88) received the B.Sc. degree in physics with electronics from the University of London, U.K., in 1974 and the Ph.D. degree in electronic engineering from the University of Bath, U.K., in 1988.

During the period 1974–1984, he worked in the scientific civil service on a number or research and development projects in the areas of communications, signal processing and EMC. Between 1984 and 1987, he worked at the University of Bath on the mathematical modelling of boxed microstrip circuits. He currently works in the Centre for Communications Research at the University of Bristol where he leads the Computational Electromagnetics team which is engaged in the development of new algorithms for electromagnetic analysis and their application to a wide variety of situations including planar and conformal antennas, microwave and RF heating systems, radar and microwave imaging, EMC, high speed interconnects and the design of photonic components.